Algorithm for the identification of resting state independent networks in fMRI

Conference Paper · January 2017

DOI: 10.1117/12.2256915

3 authors, including:

Patricio Donnelly Kehoe
National Scientific and Technical Research Cou…
7 PUBLICATIONS **0** CITATIONS
SEE PROFILE

Juan Carlos Gómez
Rosario National University
59 PUBLICATIONS **424** CITATIONS
SEE PROFILE

Algorithm for the identification of resting state independent networks in fMRI

Patricio Donnelly Kehoe[a,b], Juan Carlos Gomez[a] and Jorge Nagel[b,c]
[a]Machine Learning and Applications Group, CIFASIS-CONICET, Rosario, Argentina.
[b] Maestría en Neurociencias y Neurotecnologías, Facultad de Ciencias Médicas, Universidad Nacional de Rosario, Argentina.
[c]Neurorradiology Service, Instituto Gamma, Rosario, Argentina.

ABSTRACT

Studies have shown that the brain is constituted by anatomically segregated and functionally specific regions working in synergy as a complex network. In this context, the brain at rest does not passively retrieve environmental information and respond but instead it maintains an active representation modulated by sensory information. Using independent component analysis (ICA) over resting state recordings a discrete set of resting state networks (RSNs) has been found, which proven to be systematically present across individuals and to be modified by the state of consciousness and also in disease. ICA's main drawback is that its output consists of a series of 3D z-score maps where noise and physiological components are randomly mixed. In this work we present a computational method composed by an ICA-based noise filtering preprocessing pipeline and a template-based identification algorithm that combines spatial comparison metrics through a voting system developed to find RSNs in a subject-by-subject basis. To validate it, we use a publicly available dataset consisting of 75 resting state fMRI sessions from 25 participants scanned three different times each one. For most common RSNs the correct candidate won the voting 93% of the times and it was voted at least once in 99%. Then we probe within-subject consistency in detected RSNs by showing augmented correlation in networks from the same subject. Finally, by comparing obtained mean RSNs with the ones from nearly 30,000 participants we show that our method constitutes a personalized-medicine oriented approach to shorten the gap between RSN research and clinical applications.

Keywords: Resting state networks, fMRI, spatial pattern recognition, processing pipeline, spontaneous brain dynamics, independent component analysis

1. INTRODUCTION

The brain can be seen as a complex system where functionally and anatomically specific but highly interconnected processing sub-systems work in synergy.[1–3] From the metabolic point of view, although it only represents 2% of the body mass, it consumes approximately 20% of the total energy budget, regardless of the level of cognitive activity or sensory stimulation.[3–5] The complex neuronal connectivity of the brain and its large energy budget suggest that the brain does not passively retrieve environmental information and responds but actively maintains a representation of cognitive and behavioral responses, even when no task is being executed.[6–8]

Under this assumption the role of spontaneous activity is to maintain active representation which is modulated by sensory information. Therefore spontaneous activity should not be considered as "noise", but as a set of structured spatiotemporal profiles that reflect the functional architecture of the brain.[9]

To study this functional architecture or *functional connectivity* in which organized spatiotemporal patterns of highly correlated (and also anticorrelated) activity between distant brain regions is observed, various methods have been developed.[10–13] Using source identification algorithms over resting state fMRI recordings several studies showed that brain's spontaneous activity is spatially organized into a finite set of specific coherent patterns, called Resting State Networks (RSNs) and that these RSNs reflect the functional architecture and distribution of somatomotor, visual, auditory, attention, language and memory networks that commonly are detected during task oriented experiments.[14–16] Other studies found that some of these RSNs are also present in rats[17] and monkeys[18] and that RSNs-based features are modified by the state of consciousness[19,20] and

12th International Symposium on Medical Information Processing and Analysis, edited by Eduardo Romero, Natasha Lepore, Jorge Brieva, Ignacio Larrabide, Proc. of SPIE Vol. 10160, 101601I
 · doi: 10.1117/12.2256915

also in several diseases, including Alzheimer's disease,[21–23] Parkinson's disease,[24,25] multiple sclerosis[26] and amyotrophic lateral sclerosis.[27]

Due to these findings and given the experimental simplicity of resting state fMRI, there has been a major focus in developing processing pipelines to use RSNs for clinical applications.[28–31] Several tools to obtain RSNs have been developed, including FSL,[32–34] DPARSF[35] and REST[36] among others, as well as for post-processing and visualization like FIX[37,38] and BrainNet.[39]

A processing pipeline to retrieve RSNs starts by a preprocessing stage which usually includes imaging format conversion, initial volumes removal, motion correction, slice timing correction, skull stripping, normalization, smoothing and band-pass filtering.[40,41] Then a more specific stage is performed in which spatiotemporal patterns are analyzed using both Blood-oxygen-level dependent(BOLD) signal and voxels' coordinates.[32–36,42] One of the most commonly used methods for this step is Independent Component Analysis (ICA),[43,44] in which data is analyzed in absence of spatial bounds or prior knowledge, looking for statistical independent sources of information. Then spatial maps of groups of regions with high correlation with each independent time-signal or *component* can be drawn. Interestingly, it has been shown that ICA can extract task-related and physiological-relevant non-task-related components, as well as artifactual components.[45]

One main problem of using ICA in a subject-by-subject basis is that obtained components are not sorted in any particular manner, therefore it is difficult to use automatic techniques to explore any specific functional network searching for meaningful features. For these reasons, in this work we explore how using an ICA-based preprocessing algorithm combined with the later usage of combined spatial patterns comparison metrics can be used to detect RSNs in an effective way. To show this we analyzed the detection rate in a set of well-known RSNs as defined by Smith and collaborator in 2009,[15] where they identified 10 major consistent activation networks using both, a group ICA analysis over 36 healthy subjects and carrying out an analysis over thousands of separate activation maps from the BrainMap database, involving nearly 30,000 human subjects. The importance of proposed methods lies in the fact that it can used as a first step to develop clinical metrics using RSNs-based features.

As testing dataset we used data from a publicly available resting-state fMRI experiment where 25 participants were scanned three different times.[46] Finally, we perform an analysis looking for within-subject and between-subjects differences in the identified networks.

2. MATERIAL & METHODS

2.1 Data Set and Experimental Paradigm

A public resting state fMRI dataset available in (`http://www.nitrc.org/projects/nyu_trt/`) was used. In the experiment twenty-five participants (mean age, 29.4±8.6 years, 10 males) were scanned three times. The participants had no history of psychiatric or neurological illness, as confirmed by clinical assessment. Informed consent was obtained prior to participation. Data were collected according to protocols approved by the institutional review boards of New York University (NYU) and the NYU School of Medicine.[46]

Another public set was used consisting of RSNs maps templates from (Smith et al., 2009)[15] and (Laird et. al., 2011),[16] available in `http://fsl.fmrib.ox.ac.uk/analysis/brainmap+rsns/`. From this set we used the 10 well-matched RSN extracted from the BrainMap database, that involved nearly 30,000 human subjects.

2.2 fMRI Data Acquisition

For each participant, three resting-state scans were obtained using a Siemens Allegra 3.0 Tesla scanner. Each scan consisted of 197 contiguous echo-planar imaging (EPI) functional volumes (repetition time (TR)=2000 ms; echo time (TE)=25 ms; flip angle=90, 39 slices, matrix= 64×64; field of view (FOV)=192 mm; acquisition voxel size=$3 \times 3 \times 3mm$). Scans 2 and 3 were obtained in a single scan session, 45 min apart, between 5 and 16 months (mean, 11 ± 4 months) after scan 1. All individuals were asked to relax and remain still with their eyes open during the scan. For spatial normalization and localization, a high-resolution T1-weighted magnetization prepared gradient echo sequence was also obtained (magnetization-prepared rapid gradient-echo (MPRAGE), TR=2500 ms; TE=4.35 ms; TI=900 ms; flip angle=8; 176 slices, FOV=256 mm).[46,47]

2.3 Image Processing and Analysis

2.3.1 Preprocessing

The preprocessing was automated through Bash Scripting and was composed by three steps: Preprocessing #1, Preprocessing #2 and Preprocessing #3. After preprocessing all data, results were visually inspected to find defects in preprocessed data. The entire preprocessing pipeline is shown in Figure 1.

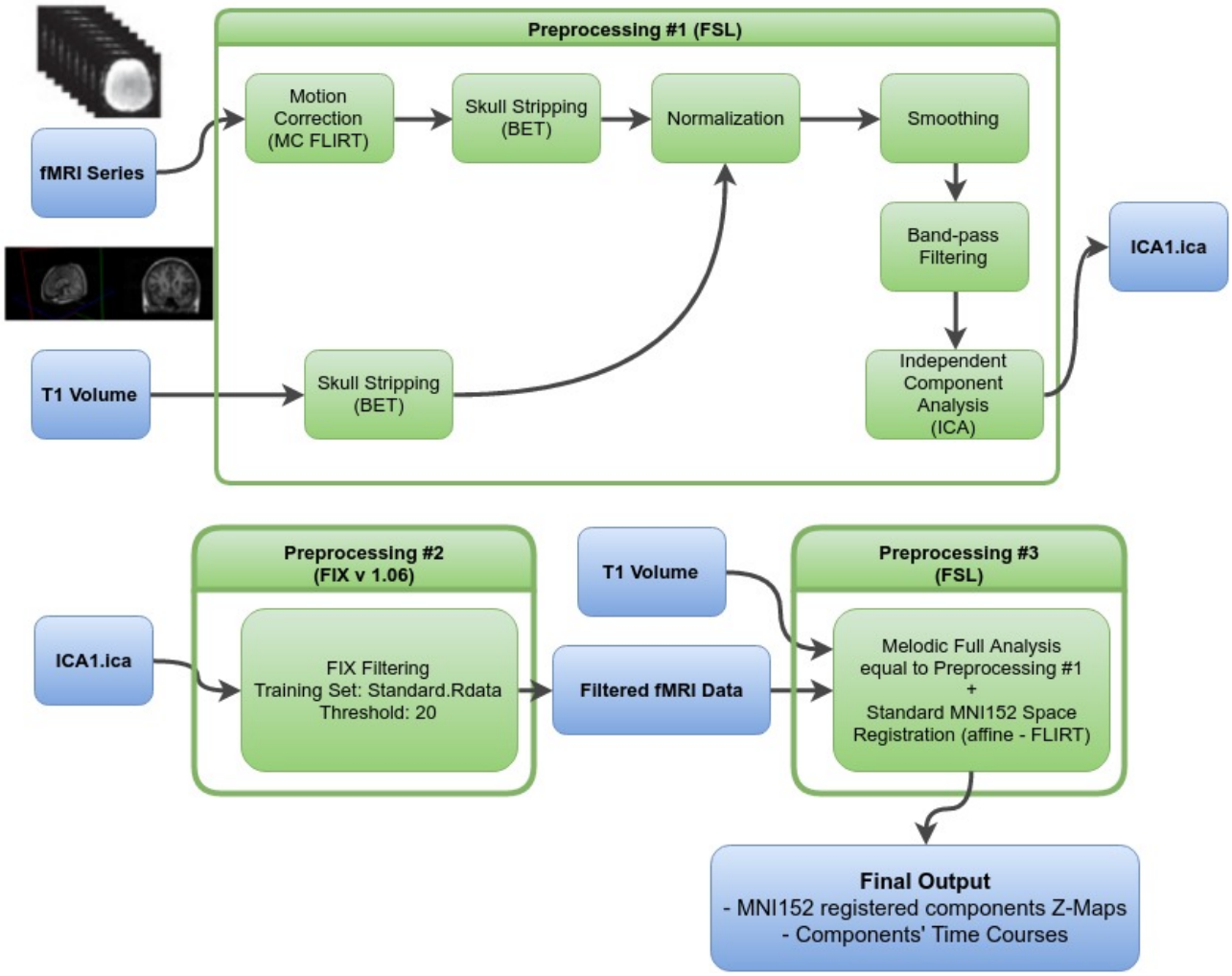

Figure 1. Flow diagram of the preprocessing pipeline. Diagram shows the flow of data and the functional blocks. Each functional containers represents stages in the preprocessing where the utilized software is shown. Boxes in blue represent packages of data while boxes in green represent sub-processes.

Step1: Preprocessing #1 fMRI data processing was carried out using FEAT (FMRI Expert Analysis Tool) Version 6.00, part of FSL (FMRIB's Software Library, `www.fmrib.ox.ac.uk/fsl`). The following pre-statistics processing was applied; motion correction using MCFLIRT;[48] non-brain removal using BET;[49] spatial smoothing using a Gaussian kernel of FWHM 5mm; grand-mean intensity normalization of the entire 4D dataset by a single multiplicative factor; high-pass temporal filtering (Gaussian-weighted least-squares straight line fitting, with sigma=50.0s). Registration to high resolution structural and/or standard space images was carried out using FLIRT.[48,50]

Components Analysis was carried out using Probabilistic Independent Component Analysis[43] as implemented in MELODIC (Multivariate Exploratory Linear Decomposition into Independent Components) Version 3.14, part of FSL (FMRIB's Software Library, `www.fmrib.ox.ac.uk/fsl`). The following data preprocessing was applied to the input data: masking of non-brain voxels; voxel-wise de-meaning of the data; normalization of the voxel-wise variance; Preprocessed data was whitened and projected into a N-dimensional subspace using probabilistic Principal Component Analysis where the number of dimensions (N) was estimated using the Laplace approximation to the Bayesian evidence of the model order.[43,51] The whitened observations were decomposed into sets of vectors which describe signal variation across the temporal domain (time-courses) and across the spatial domain (maps) by optimizing for non-Gaussian spatial source distributions using a fixed-point iteration technique.[52] Estimated Component maps were divided by the standard deviation of the residual noise and thresholded by fitting a mixture model to the histogram of intensity values.[43]

Step 2: Preprocessing #2 Using Preprocessing #1 output (ICA1.ica in Figure 1) an automatic denoising of functional MRI data was performed by combining independent component analysis and hierarchical fusion of classifiers using MRIB's ICA-based Xnoiseifier (FIX) v1.061 Beta.[37,38] We have used the Standard.RData training set and a value of 20 as the threshold (for more information see `http://fsl.fmrib.ox.ac.uk/fsl/fslwiki/FIX`).

Step 3: Preprocessing #3 Using the denoised fMRI data (Preprocessing #2 output) a similar pipeline to Preprocessing #1 ICA analysis was used but with a fixed number of 20 components. Finally resulting Z-score maps were registered to Standard MNI152 Space[53] using FMRIB's Linear Image Registration Tool (FLIRT)[48,50] with an affine transformation, using as work flow [low resolution Image]->[structural Image]->[reference image]. The final output was the set [Registered-Z-Maps]+[component's time-signals].

2.3.2 Standard Components Identification

The Standard component extraction was implemented using the statistical programming language R[54] and was divided in several steps, schematically depicted in Figure 2. All the .nii.gz extension files were read from inside R using AnalyzeFMRI R Package.[55]

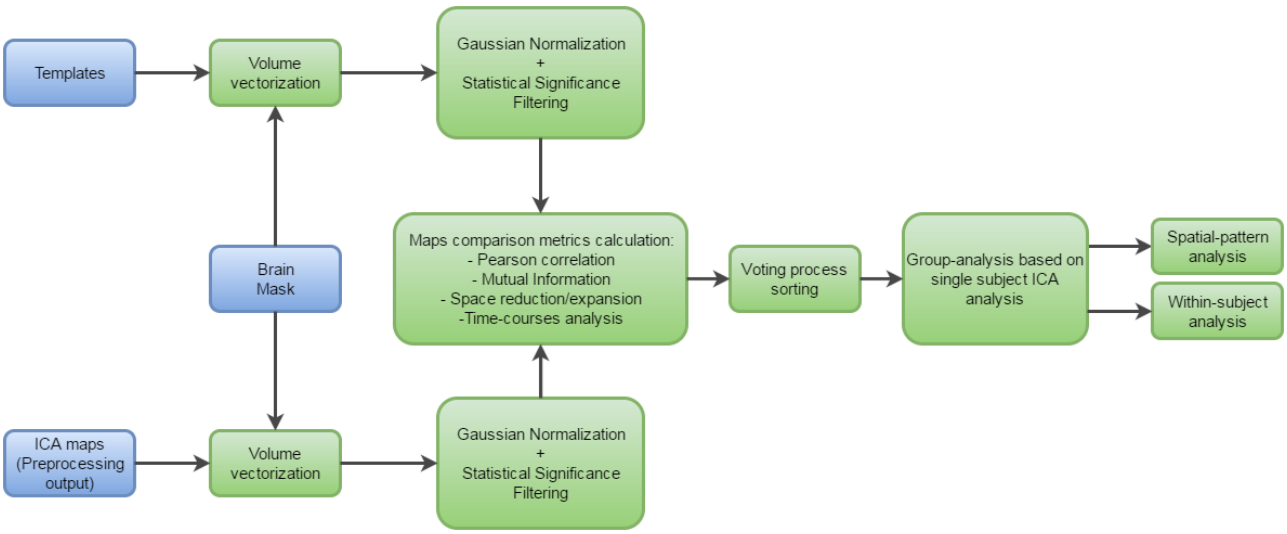

Figure 2. Flow diagram of the processing pipeline. Diagram shows the flow of data and the functional blocks. Boxes in blue represent packages of data while boxes in green processing and analysis stages.

Mask definition A representative brain mask was defined using standard MNI152 template data.[53] The mask was obtained extracting eyes and ventricles from the original brain mask helping to reduce the influence of no-activity regions.

Volume vectorization Templates Z-Maps and Components Z-maps were vectorized accordingly to the mask to achieve voxel-wise spatial matching.

Gaussian normalization and Statistical Significance filtering In this step vectorized maps and templates were statistically processed based on (Wang & Peterson, 2008).[56] First we normalized to have zero mean and unit variance (normal Gaussian distribution). Let IC_i denote the ith independent component and M_Z^i denote its Z-score map. The normalization process can be express as:

$$M_Z^i = (IC_i - mean(IC_i))/std(IC_i)$$

Later on, each M_Z^i has been filtered according to the following rule:

$$\mathbf{M}_Z^i(x,y,z) = \begin{cases} M_Z^i(x,y,z): & \text{if } \mid M_Z^i(x,y,z) \mid \geq Z_T \\ Z_L: & \text{if } M_Z^i(x,y,z) \leq Z_L \\ Z_U: & \text{if } M_Z^i(x,y,z) \geq Z_U \\ 0: & \text{otherwise} \end{cases}$$

We set $Z_T = 1.96$ (corresponding to a p-value < 0.05), $Z_U = 6$ and $Z_L = -6$ (both corresponding to sufficiently significant p-values $< 5 \times 10^{-9}$).

Selection of most similar patterns To match component's maps with RSNs templates the following metrics were used:

- *Pearson Correlation Coefficient:* implemented using Stats R Package.
- *Mutual Information Coefficient:* Using a discretization version of each map we used the R Package 'infotheo' to calculate the mutual information score.
- *Space reduction/expansion:* Both Pearson Correlation and Mutual Information coefficients were calculated several times (three times for correlation and two for mutual information). These different calculations were made by using a new concept developed in this article, called space reduction and space expansion. Reduced space is considered the one that includes only voxels in which the value differs from 0 in one of the two compared volumes. This volume that is taken as reference is considered the center of the operation. So if for example we have two z-score maps, the component (C) and the template (T) and we compare them using the reduced correlation that considers only voxels other than 0 in T, it will be called *reduced correlation centered in T* and written as $rCor(T)$.
  Expanded space is the one that includes all voxels that are not zero in the template *or* in the proposed subject z-score map.

After a series of preliminary tests, 5 comparisons coefficients have been selected and named according to the process:

- *rCor(T) (reduced correlation centered in the template):* this operation calculates the Pearson Correlation Index between the component and the template, considering only elements that are not zero in the template(T).
- *eCor (expanded correlation):* this operation calculates the Pearson Correlation Index between a two vectors considering elements that are not zero in the template or in the proposed component.

- *rCor(C) (reduced correlation centered in the component):* this operation calculates the Pearson Correlation Index between the component and the template, considering only elements that are not zero in the proposed component(C).
- *rMI(T) (reduced Mutual Information centered in the template):* this operation calculates the Mutual Information Index between the component and the template, considering only elements that are not zero in the template(T).
- *rMI(C) (reduced Mutual Information centered in the component):* this operation calculates the Mutual Information Index between the component and the template, considering only elements that are not zero in the proposed component(C).

After some preliminary tests, it was decided to give 1.5 points for the winner of the rCor(T) index and 1 point for the winners of the other indexes, so the rCor(T) index would have priority in case that all indexes give different maps as a winner.
After computing a voting score for the matching between subjects component and standard templates, components were sorted according to these template correspondence.[15]

To validate the computerized identification, a manual matching between components and standard templates was made, resulting in a truth table. Therefore, each of the 75 set of components was matched to the standard templates (if possible). When not even one of the 20 components matched a template, it was marked as not found.

Analysis of the selection process Three analyses were performed to validate the detection algorithm:

- *Level of matching with the truth table (TT):* it was made to know how many components were correctly selected, how many were suggested (voted by at least one or more comparison coefficient, but not winner in the voting process) and how many errors the algorithm was making (not even voting one time the correct component).
- *Spatial pattern analysis:* it was made to establish if the mean pattern of the groups were similar to the RSN patterns used. Additionally, it was quantified to what extent each selected RSNs was correlated with its matching template.
- *Within-subject Analysis:* the objective of this test was to measure to what extent the "same" RSN was detected in a single subject for multiples runs and at different times.

3. RESULTS

3.1 Preprocessing

As mentioned before the complete preprocessing pipeline was automated using a bash scripting. All the registries in the dataset (N=75) were processed satisfactory after visual verification of each one using FSL View Software. Therefore it can be affirmed that the processing automation has been satisfactorily implemented.

3.2 Processing

3.2.1 Construction of the TT

The overall matching between components and RSNs templates is shown in Figure 3, where RSNs according to Smith et. al. are listed in the x-axis[15] and in the y-axis is represented the number of times each network was found in the output of the processing pipeline. RSN #1 and RSN #4 were found in most recordings, while RSN #5 and RSN #3 were the least found. Also it can be noticed that final N was 74, given that due to excessive noise one fMRI recording was excluded. As expected the RSN related to the primary visual area (RSN #1) was present in all recordings and default mode network (RSN #4) could not be found in only two of them. On the other hand, cerebellum network (RSN #5) was found in only 32 of the 74 records. As for RSN #2 and

RSN #3, they have an overlapping both functionally and spatially with RSN #1, as they are all related with the visual processing and in some cases these networks were clustered in one big component. Is for this reason that many times RSN #2 and RSN #3 were not found. RSN #8 is spatially overlapped with RSN #4, RSN #9 and RSN #10, and we believe that for this reason it was found in only 58 times.

3.2.2 Standard RSNs detection

After construction of the truth table and taking into account the observations made in the process, we first analyzed reference RSNs to detect possible spatial and functional correlations between them or if there was any problematic from the technical perspective. We decided not to excluded any network from the results but to define a priority subgroup for the subsequent analyses. Hence, we decided to exclude RSNs #2,#3,#5,#8 from thorough analyses. RSNs #2 and #3 were excluded because of the high spatial and functional correlation with RSN #1, RSN #5 was excluded because the cerebellum is not always scanned and finally RSN #8 because was not encountered frequently in the visual inspection and also because of the highly spatial correlation with #4,#6, #9 and #10. Therefore, selected templates for further analysis were #1 (Visual Network),#4 (Default Mode Network), #6 (Temporo-Parietal Network), #7 (Auditory Network), #9 (Right Fronto-Parietal Network) and #10 (Left Fronto-Parietal Network). In the analyses of the detection algorithm two possible cases were taken into account. i) One network was considered as *suggested* when the correct component (the manually selected) has received at least one vote, without winning the voting process and ii) a network was considered as *correctly selected* when the correct component won the voting process. These two categories were considered to analyze the possibility of using the method in a semi-automated RSNs detection system, where the user has the chance to finally select which component best represents each particular RSN. Results for the computerized identification for each RSN are shown in Figure 3, where it should be noticed that for most relevant RSNs, namely #1, #4, #6, #7, #9 and #10, the overall rate of correctly selected was very high with a maximum of 98,6% in the case of RSN #1 and a minimum of 85% in the case of RSN #6. As for the suggestion rate in the same group of RSNs the maximum have been 100% for RSNs #1, #4, #6 and #9, while the minimum was observed in RSN #7 with 96.9%.

Table 1 shows the mean rCor(T) value for the winner component in cases where the searched RSN was present and when it was not. As can be seen the value of rCor(T) doubled the value when the the RSN was present between candidates, suggesting that this coefficient can be used not only to select look for the best candidate, but also to detect if the searched RSN is even present. Statistical significance could not be calculated because of small number of $notfoundRSNs$ for relevant networks.

	RSN1	**RSN2**	**RSN3**	**RSN4**	**RSN5**	**RSN6**	**RSN7**	**RSN8**	**RSN9**	**RSN10**
Found Components Mean rCor(T)	0.51	0.43	0.27	0.49	0.27	0.26	0.33	0.32	0.36	0.38
Found Components SD rCor(T)	0.11	0.15	0.12	0.09	0.15	0.15	0.1	0.11	0.07	0.13
Not-Found Components Mean rCor(T)	—	0.23	0.12	0.11	0.12	0.14	0.17	0.20	0.24	0.17
% Difference	—	47	56	78	56	46	48	38	33	55

Table 1. Differences in mean *rCor(T)* metric of the winner candidate in sets when the RSN was *Found* and *Not-Found*.

3.2.3 Level of matching with the TT

Figure 4 shows how effective each metric was in detecting the right component. In overall, the best comparison metric was rCor(T), followed by rMI(T), rCorr(C), rMI(C) and finally eCorr, suggesting that expanded methods are not effective for RSNs detection using spatial maps. As can be noticed in the figure, for most cases the voting result exhibited better performance than the most accurate metric. For example, in the case of Default Mode Network (RSN #4) the most accurate metric was rCorr(T) with 63 out of 72 correct identifications, while the overall efficacy of the voting process was 71 out of 72.

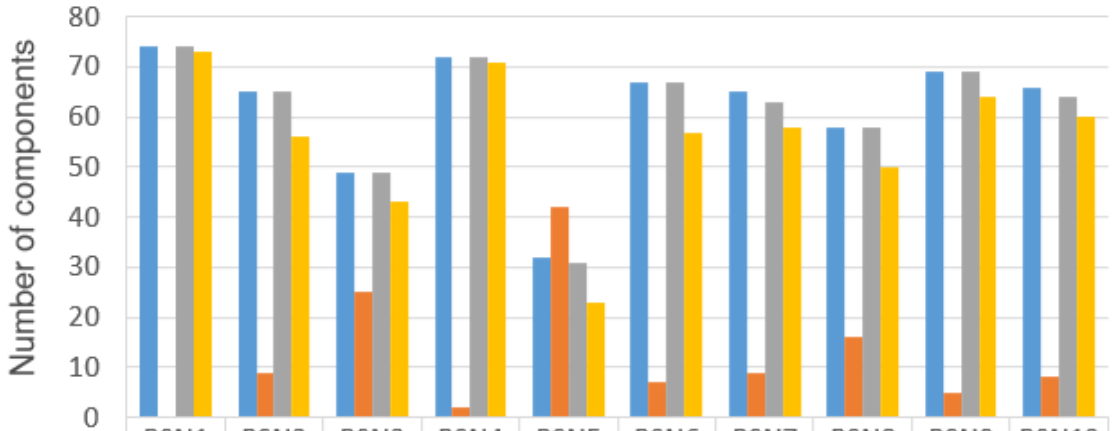

	RSN1	RSN2	RSN3	RSN4	RSN5	RSN6	RSN7	RSN8	RSN9	RSN10
Found Components	74	65	49	72	32	67	65	58	69	66
Not found	0	9	25	2	42	7	9	16	5	8
Suggested	74	65	49	72	31	67	63	58	69	64
Correctly Selected	73	56	43	71	23	57	58	50	64	60

Figure 3. Visual inspection detection versus computerized identification performance. Comparison between the visual matching and computerized selection where *Found components* refers to how many times each RSN was found in the ICA output *by visual inspection*. *Not found* are the number of times that each RSN was not found *by visual inspection*. *Suggested* indicates how many times the selected component by visual inspection was voted at least once in the computerized identification. *Correct Selected* is the number of times that the correct component won the voting process.

3.2.4 Within-subject Analysis

An spatial analysis was made to assess for within-subject consistency by comparing the resemblance of RSNs from the same subject obtained in multiple resting state sessions with the resemblance of all detected RSNs (between-subjects). To quantify this spatial coincidence between two maps a *mean reduced correlation coefficient* was used, therefore similarity between spatial maps A and B was compute as $(rCor(A)+rCor(B))/2$. In Table 2 are shown the results from the within-subject analysis where it should be noticed that significant differences were found for all RSNs of interest, with higher scores of correlation between networks from the same subject, showing that although spatial distribution of RSNs are similar across subjects the resemblance between acquisition runs in the same subject is significantly higher.

# RSN	**#1**	**#4**	**#6**	**#7**	**#9**	**#10**
mean Self-Correlation (N)	0.56 (71)	0.41 (67)	0.31 (45)	0.31 (46)	0.47 (56)	0.36(47)
sd Self-Correlation	0.177	0.154	0.184	0.155	0.142	0.17
mean All-Correlation (N)	0.44* (2628)	0.31* (2485)	0.21** (1596)	0.20* (1653)	0.28* (2016)	0.23* (1770)
sd All-Correlation	0.14	0.10	0.125	0.088	0.08	0.092

(*) Two samples are significantly different according to t-test (alpha = 0.01; two-sided; $p<0.0001$)
(**) Two samples are significantly different according to t-test (alpha = 0.01; two-sided; $p<0.001$)
Table 2. Within-Subject Analysis. Comparison between mean reduced correlation using networks from the same subject and networks from different subjects for each RSN of interest.

3.2.5 Mean RSNs

As a final result we obtained subject-by-subject based mean RSNs for each of the 6 RSNs of interest. Figures 5 to 7 show that mean RSNs obtained by our *group analysis based on single subject's ICA* are very similar

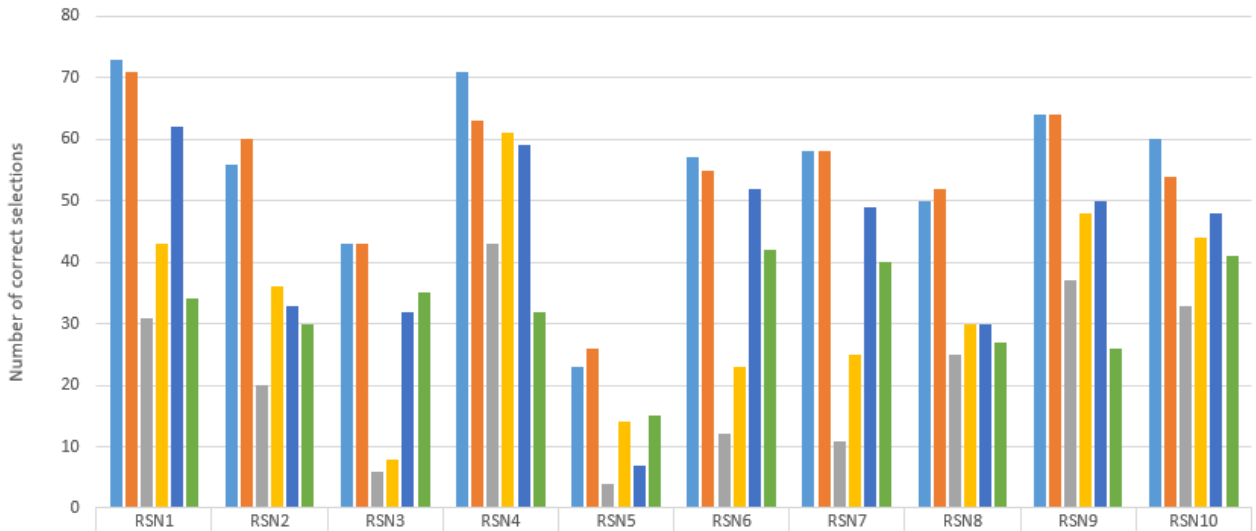

	RSN1	RSN2	RSN3	RSN4	RSN5	RSN6	RSN7	RSN8	RSN9	RSN10
Voting	73	56	43	71	23	57	58	50	64	60
rCorr(T)	71	60	43	63	26	55	58	52	64	54
eCorr	31	20	6	43	4	12	11	25	37	33
rCorr(C)	43	36	8	61	14	23	25	30	48	44
rMI(T)	62	33	32	59	7	52	49	30	50	48
rMI(C)	34	30	35	32	15	42	40	27	26	41

Figure 4. Individual metric usage versus combined performance. Bar plot shows the number of correct identifications for each metric. It should be noticed that for each RSN the maximum number of found components depends on the number of times it was detected by visual inspection (shown in Figure 3).

to the ones obtained by (Smith et al., 2009)[15] using group ICA. This suggest that our method can allow a subject-by-subject based RSN analysis closing the gap between resting state fmri and its clinical applications.

4. CONCLUSION

We designed and tested a pipeline to obtain filtered and categorized RSNs in a subject-by-subject basis according to a set of RSN templates. The method was tested in a dataset consisting of 75 resting state fMRI recordings and showed robustness in cases where the searched RSN was present in the ICA's output. A remaining challenge is the identification of whether a particular RSN is present in ICA's output or not. With this aim the algorithm could be complemented by the user interaction as part of a suggestion system. In this line, results showed that for the common RSNs (#1, #4, #6, #7, #9 and #10) over 99% (409 out of 413) of the components were suggested and in the 93% of the cases the winner of the voting process was the correct one. For these reasons using the presented preprocessing pipeline combined by the subsequent identification algorithm can potentially save time and efforts when trying to isolate a set of RSNs in large datasets.

In the matter of finding if a RSN is or not in the preprocessing output, reduce correlation metric showed that the winner component is much larger when the RSN is between the candidates that when it is not although significance could not be measure because the cases where these RSNs where not found was too small.

We also analyzed which of the proposed similarity metrics were more useful, showing that expanded comparison indexes have worst performance that reduced ones and that template centered metrics were presented a better performance that candidate centered ones. Nevertheless, the combined use of all metrics in a voting process probed to most accurate than any of them separately.

In order to asses for within-subject consistency we conducted a spatial analysis, founding that within-subject similarity between RSN distribution maps obtained in different fMRI sessions was significantly higher than between-subjects spatial correlation of RSNs.

Finally, mean group RSNs obtained using the proposed method showed a similar spatial patterns to the ones

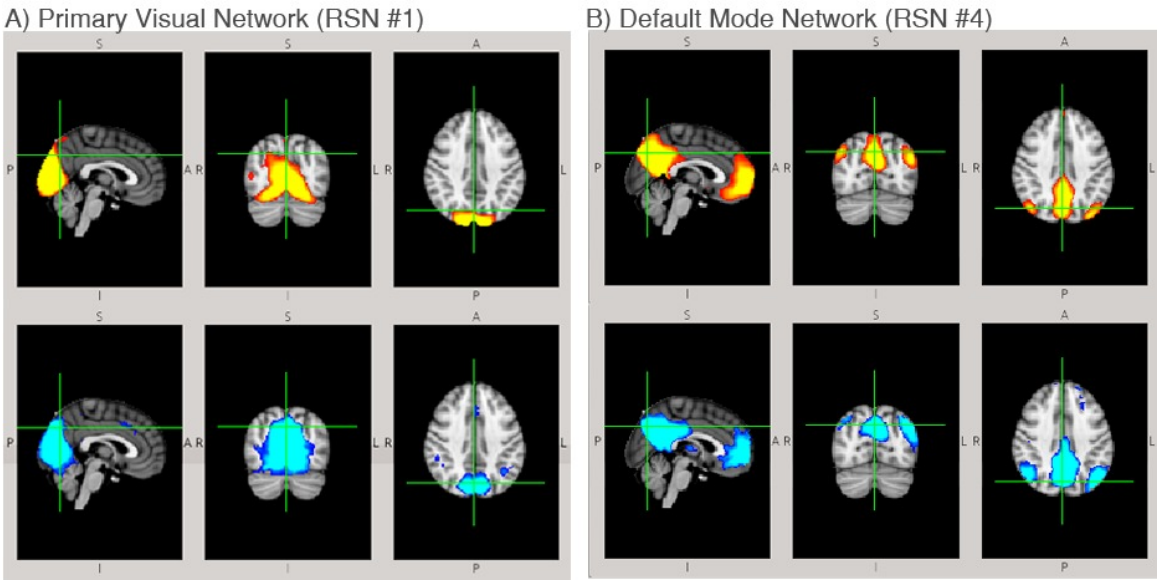

Figure 5. Comparison between mean RSNs obtained by our subject-by-subject based processing pipeline (upper image in red-yellow scale) and the corresponding group-ICA based homologous published by (Smith et al., 2009)[15] (bottom image in blue-light blue scale). In A) Primary Visual Network (RSN #1) and in B) Default Mode Network (RSN #4).

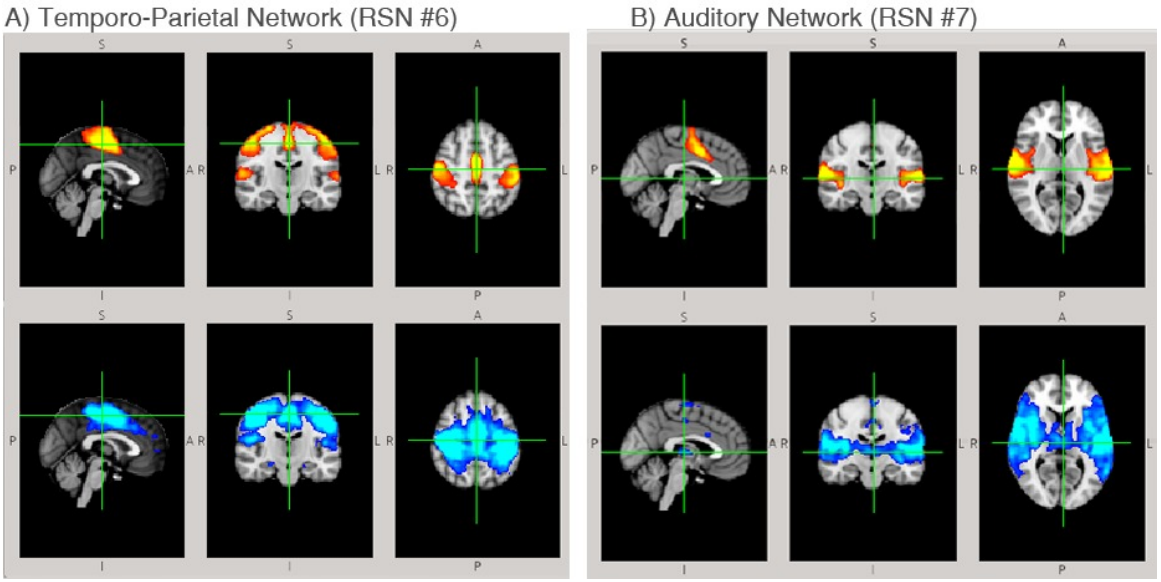

Figure 6. Comparison between mean RSNs obtained by our subject-by-subject based processing pipeline (upper image in red-yellow scale) and the corresponding group-ICA based homologous published by (Smith et al., 2009)[15] (bottom image in blue-light blue scale). In A) Parieto-temporal Network (RSN #6) and in B) Auditory Network (RSN #7).

found by Smith and collaborators[15] using group ICA analysis, suggesting that it is possible to use more individualized-medicine oriented approaches to retrieve RSNs that can shorten the gap between resting state networks research and its clinical applications.

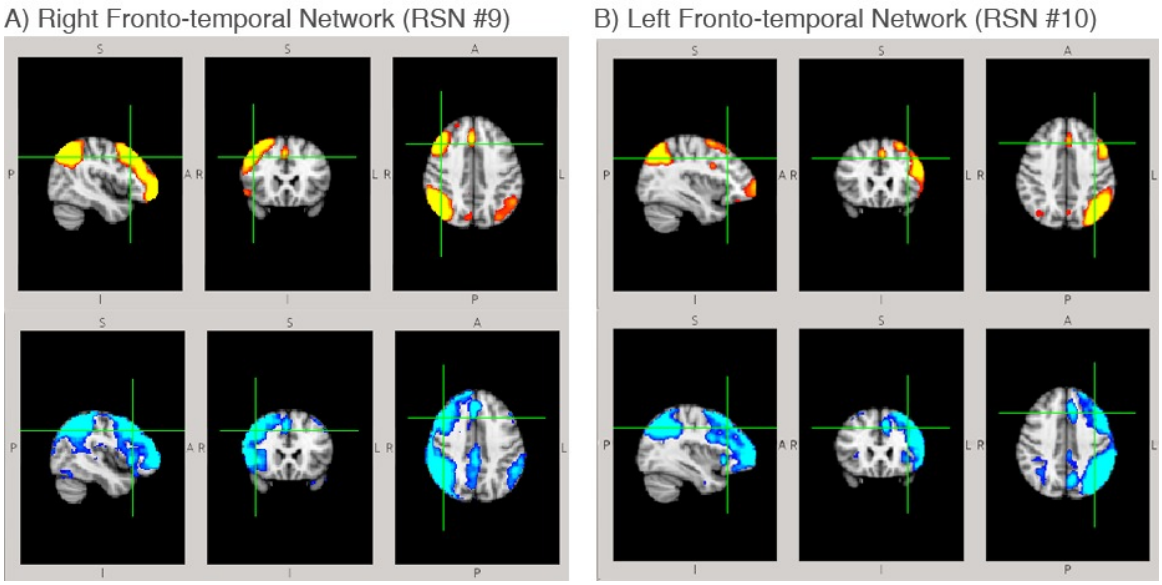

Figure 7. Comparison between mean RSNs obtained by our subject-by-subject based processing pipeline (upper image in red-yellow scale) and the corresponding group-ICA based homologous published by (Smith et al., 2009)[15] (bottom image in blue-light blue scale).In A) Right Fronto-temporal Network (RSN #9) and in B) Left Fronto-temporal Network (RSN #10).

REFERENCES

[1] Varela, F., Lachaux, J.-P., Rodriguez, E., and Martinerie, J., "The brainweb: phase synchronization and large-scale integration," *Nature reviews neuroscience* **2**(4), 229–239 (2001).

[2] Buzsáki, G. and Draguhn, A., "Neuronal oscillations in cortical networks," *science* **304**(5679), 1926–1929 (2004).

[3] Hagmann, P., Cammoun, L., Gigandet, X., Meuli, R., Honey, C. J., Wedeen, V. J., and Sporns, O., "Mapping the structural core of human cerebral cortex," *PLoS Biol* **6**(7), e159 (2008).

[4] Gusnard, D. A. and Raichle, M. E., "Searching for a baseline: functional imaging and the resting human brain," *Nature Reviews Neuroscience* **2**(10), 685–694 (2001).

[5] Raichle, M. E. and Gusnard, D. A., "Appraising the brain's energy budget," *Proceedings of the National Academy of Sciences* **99**(16), 10237–10239 (2002).

[6] Engel, A. K., Fries, P., and Singer, W., "Dynamic predictions: oscillations and synchrony in top–down processing," *Nature Reviews Neuroscience* **2**(10), 704–716 (2001).

[7] Fox, M. D. and Raichle, M. E., "Spontaneous fluctuations in brain activity observed with functional magnetic resonance imaging," *Nature Reviews Neuroscience* **8**(9), 700–711 (2007).

[8] Gillebert, C. R. and Mantini, D., "Functional connectivity in the normal and injured brain," *The Neuroscientist* **19**(5), 509–522 (2013).

[9] Deco, G. and Corbetta, M., "The dynamical balance of the brain at rest," *The Neuroscientist* **17**(1), 107–123 (2011).

[10] Biswal, B., Zerrin Yetkin, F., Haughton, V. M., and Hyde, J. S., "Functional connectivity in the motor cortex of resting human brain using echo-planar mri," *Magnetic resonance in medicine* **34**(4), 537–541 (1995).

[11] Fox, M. D., Snyder, A. Z., Vincent, J. L., Corbetta, M., Van Essen, D. C., and Raichle, M. E., "The human brain is intrinsically organized into dynamic, anticorrelated functional networks," *Proceedings of the National Academy of Sciences of the United States of America* **102**(27), 9673–9678 (2005).

[12] Fox, M. D., Snyder, A. Z., Zacks, J. M., and Raichle, M. E., "Coherent spontaneous activity accounts for trial-to-trial variability in human evoked brain responses," *Nature neuroscience* **9**(1), 23–25 (2006).

[13] De Luca, M., Beckmann, C., De Stefano, N., Matthews, P., and Smith, S. M., "fmri resting state networks define distinct modes of long-distance interactions in the human brain," *Neuroimage* **29**(4), 1359–1367 (2006).

[14] Damoiseaux, J., Rombouts, S., Barkhof, F., Scheltens, P., Stam, C., Smith, S. M., and Beckmann, C., "Consistent resting-state networks across healthy subjects," *Proceedings of the national academy of sciences* **103**(37), 13848–13853 (2006).

[15] Smith, S. M., Fox, P. T., Miller, K. L., Glahn, D. C., Fox, P. M., Mackay, C. E., Filippini, N., Watkins, K. E., Toro, R., Laird, A. R., et al., "Correspondence of the brain's functional architecture during activation and rest," *Proceedings of the National Academy of Sciences* **106**(31), 13040–13045 (2009).

[16] Laird, A. R., Fox, P. M., Eickhoff, S. B., Turner, J. A., Ray, K. L., McKay, D. R., Glahn, D. C., Beckmann, C. F., Smith, S. M., and Fox, P. T., "Behavioral interpretations of intrinsic connectivity networks," *Journal of cognitive neuroscience* **23**(12), 4022–4037 (2011).

[17] Lu, H., Zou, Q., Gu, H., Raichle, M. E., Stein, E. A., and Yang, Y., "Rat brains also have a default mode network," *Proceedings of the National Academy of Sciences* **109**(10), 3979–3984 (2012).

[18] Vincent, J., Patel, G., Fox, M., Snyder, A., Baker, J., Van Essen, D., Zempel, J., Snyder, L., Corbetta, M., and Raichle, M., "Intrinsic functional architecture in the anaesthetized monkey brain," *Nature* **447**(7140), 83–86 (2007).

[19] Boveroux, P., Vanhaudenhuyse, A., Bruno, M.-A., Noirhomme, Q., Lauwick, S., Luxen, A., Degueldre, C., Plenevaux, A., Schnakers, C., Phillips, C., et al., "Breakdown of within-and between-network resting state functional magnetic resonance imaging connectivity during propofol-induced loss of consciousness," *The Journal of the American Society of Anesthesiologists* **113**(5), 1038–1053 (2010).

[20] Heine, L., Soddu, A., Gómez, F., Vanhaudenhuyse, A., Tshibanda, L., Thonnard, M., Charland-Verville, V., Kirsch, M., Laureys, S., and Demertzi, A., "Resting state networks and consciousness," *Frontiers in psychology* **3**, 295 (2012).

[21] Rombouts, S. A., Barkhof, F., Goekoop, R., Stam, C. J., and Scheltens, P., "Altered resting state networks in mild cognitive impairment and mild alzheimer's disease: an fmri study," *Human brain mapping* **26**(4), 231–239 (2005).

[22] Sorg, C., Riedl, V., Mühlau, M., Calhoun, V. D., Eichele, T., Läer, L., Drzezga, A., Förstl, H., Kurz, A., Zimmer, C., et al., "Selective changes of resting-state networks in individuals at risk for alzheimer's disease," *Proceedings of the National Academy of Sciences* **104**(47), 18760–18765 (2007).

[23] Sanz-Arigita, E. J., Schoonheim, M. M., Damoiseaux, J. S., Rombouts, S. A., Maris, E., Barkhof, F., Scheltens, P., and Stam, C. J., "Loss of small-worldnetworks in alzheimer's disease: graph analysis of fmri resting-state functional connectivity," *PloS one* **5**(11), e13788 (2010).

[24] Wu, T., Wang, L., Chen, Y., Zhao, C., Li, K., and Chan, P., "Changes of functional connectivity of the motor network in the resting state in parkinson's disease," *Neuroscience letters* **460**(1), 6–10 (2009).

[25] Tessitore, A., Amboni, M., Esposito, F., Russo, A., Picillo, M., Marcuccio, L., Pellecchia, M. T., Vitale, C., Cirillo, M., Tedeschi, G., et al., "Resting-state brain connectivity in patients with parkinson's disease and freezing of gait," *Parkinsonism & related disorders* **18**(6), 781–787 (2012).

[26] Bonavita, S., Gallo, A., Sacco, R., Della Corte, M., Bisecco, A., Docimo, R., Lavorgna, L., Corbo, D., Di Costanzo, A., Tortora, F., et al., "Distributed changes in default-mode resting-state connectivity in multiple sclerosis," *Multiple sclerosis journal* **17**(4), 411–422 (2011).

[27] Mohammadi, B., Kollewe, K., Samii, A., Krampfl, K., Dengler, R., and Münte, T. F., "Changes of resting state brain networks in amyotrophic lateral sclerosis," *Experimental neurology* **217**(1), 147–153 (2009).

[28] Matthews, P. M., Honey, G. D., and Bullmore, E. T., "Applications of fmri in translational medicine and clinical practice," *Nature Reviews Neuroscience* **7**(9), 732–744 (2006).

[29] Fox, M. D. and Raichle, M. E., "Spontaneous fluctuations in brain activity observed with functional magnetic resonance imaging," *Nature Reviews Neuroscience* **8**(9), 700–711 (2007).

[30] Fox, M. D. and Greicius, M., "Clinical applications of resting state functional connectivity," *Front Syst Neurosci* **4**, 19 (2010).

[31] Rosazza, C. and Minati, L., "Resting-state brain networks: literature review and clinical applications," *Neurological Sciences* **32**(5), 773–785 (2011).

[32] Smith, S. M., Jenkinson, M., Woolrich, M. W., Beckmann, C. F., Behrens, T. E., Johansen-Berg, H., Bannister, P. R., De Luca, M., Drobnjak, I., Flitney, D. E., Niazy, R. K., Saunders, J., Vickers, J., Zhang, Y., De Stefano, N., Brady, J. M., and Matthews, P. M., "Advances in functional and structural MR image analysis and implementation as FSL," *Neuroimage* **23 Suppl 1**, S208–219 (2004).

[33] Woolrich, M. W., Jbabdi, S., Patenaude, B., Chappell, M., Makni, S., Behrens, T., Beckmann, C., Jenkinson, M., and Smith, S. M., "Bayesian analysis of neuroimaging data in fsl," *Neuroimage* **45**(1), S173–S186 (2009).

[34] Jenkinson, M., Beckmann, C. F., Behrens, T. E., Woolrich, M. W., and Smith, S. M., "Fsl," *Neuroimage* **62**(2), 782–790 (2012).

[35] Chao-Gan, Y. and Yu-Feng, Z., "Dparsf: a matlab toolbox for pipeline data analysis of resting-state fmri," *Frontiers in systems neuroscience* **4** (2010).

[36] Song, X.-W., Dong, Z.-Y., Long, X.-Y., Li, S.-F., Zuo, X.-N., Zhu, C.-Z., He, Y., Yan, C.-G., and Zang, Y.-F., "Rest: a toolkit for resting-state functional magnetic resonance imaging data processing," *PloS one* **6**(9), e25031 (2011).

[37] Salimi-Khorshidi, G., Douaud, G., Beckmann, C. F., Glasser, M. F., Griffanti, L., and Smith, S. M., "Automatic denoising of functional mri data: combining independent component analysis and hierarchical fusion of classifiers," *Neuroimage* **90**, 449–468 (2014).

[38] Griffanti, L., Salimi-Khorshidi, G., Beckmann, C. F., Auerbach, E. J., Douaud, G., Sexton, C. E., Zsoldos, E., Ebmeier, K. P., Filippini, N., Mackay, C. E., et al., "Ica-based artefact removal and accelerated fmri acquisition for improved resting state network imaging," *Neuroimage* **95**, 232–247 (2014).

[39] Xia, M., Wang, J., and He, Y., "Brainnet viewer: a network visualization tool for human brain connectomics," *PloS one* **8**(7), e68910 (2013).

[40] Gargouri, F., Delphine, S., Lehéricy, S., and Hamida, A. B., "The influence of preprocessing steps on functional connectivity in resting state fmri," in [*2016 2nd International Conference on Advanced Technologies for Signal and Image Processing (ATSIP)*], 103–107, IEEE (2016).

[41] Vergara, V. M., Mayer, A. R., Damaraju, E., Hutchison, K., and Calhoun, V. D., "The effect of preprocessing pipelines in subject classification and detection of abnormal resting state functional network connectivity using group ica," *NeuroImage* (2016).

[42] Yan, C.-G., Wang, X.-D., Zuo, X.-N., and Zang, Y.-F., "Dpabi: Data processing & analysis for (resting-state) brain imaging," *Neuroinformatics* , 1–13 (2016).

[43] Beckmann, C. F. and Smith, S. M., "Probabilistic independent component analysis for functional magnetic resonance imaging," *IEEE transactions on medical imaging* **23**(2), 137–152 (2004).

[44] Beckmann, C. F., DeLuca, M., Devlin, J. T., and Smith, S. M., "Investigations into resting-state connectivity using independent component analysis," *Philosophical Transactions of the Royal Society of London B: Biological Sciences* **360**(1457), 1001–1013 (2005).

[45] Storti, S. F., Formaggio, E., Nordio, R., Manganotti, P., Fiaschi, A., Bertoldo, A., and Toffolo, G. M., "Automatic selection of resting-state networks with functional magnetic resonance imaging," *Front Neurosci* **7**, 1–10 (2013).

[46] Shehzad, Z., Kelly, A. C., Reiss, P. T., Gee, D. G., Gotimer, K., Uddin, L. Q., Lee, S. H., Margulies, D. S., Roy, A. K., Biswal, B. B., et al., "The resting brain: unconstrained yet reliable," *Cerebral cortex* **19**(10), 2209–2229 (2009).

[47] Zuo, X.-N., Di Martino, A., Kelly, C., Shehzad, Z. E., Gee, D. G., Klein, D. F., Castellanos, F. X., Biswal, B. B., and Milham, M. P., "The oscillating brain: complex and reliable," *Neuroimage* **49**(2), 1432–1445 (2010).

[48] Jenkinson, M., Bannister, P., Brady, M., and Smith, S., "Improved optimization for the robust and accurate linear registration and motion correction of brain images," *Neuroimage* **17**(2), 825–841 (2002).

[49] Smith, S. M., "Fast robust automated brain extraction," *Human brain mapping* **17**(3), 143–155 (2002).

[50] Jenkinson, M. and Smith, S., "A global optimisation method for robust affine registration of brain images," *Medical image analysis* **5**(2), 143–156 (2001).

[51] Minka, T. P., "Automatic choice of dimensionality for pca," in [*NIPS*], **13**, 598–604 (2000).

[52] Hyvarinen, A., "Fast and robust fixed-point algorithms for independent component analysis," *IEEE Trans Neural Netw* **10**(3), 626–634 (1999).

[53] Grabner, G., Janke, A. L., Budge, M. M., Smith, D., Pruessner, J., and Collins, D. L., "Symmetric atlasing and model based segmentation: an application to the hippocampus in older adults," *Med Image Comput Comput Assist Interv* **9**(Pt 2), 58–66 (2006).

[54] R Development Core Team, *R: A Language and Environment for Statistical Computing*. R Foundation for Statistical Computing, Vienna, Austria (2008). ISBN 3-900051-07-0.

[55] Bordier, C., Dojat, M., and de Micheaux, P. L., "Temporal and spatial independent component analysis for fmri data sets embedded in the AnalyzeFMRI R package," *Journal of Statistical Software* **44**(9), 1–24 (2011).

[56] Wang, Z. and Peterson, B. S., "Partner-matching for the automated identification of reproducible ICA components from fMRI datasets: algorithm and validation," *Hum Brain Mapp* **29**(8), 875–893 (2008).